Optimization of Spatial Morphology and Wall Construction Parameters of Double-Sided Solar Greenhouses Based on CFD

Haoyue Wang , Hengyu Tan , Zhuohuan Li , Yunfei Ma *

Posted Date: 7 May 2026

doi: 10.20944/preprints202605.0411.v1

Keywords: double-sided solar greenhouse; CFD simulation; spatial morphology optimization; photothermal environment; facility agriculture

 doi:10.20944/preprints202605.0411.v1

Article

Optimization of Spatial Morphology and Wall Construction Parameters of Double-Sided Solar Greenhouses Based on CFD

Haoyue Wang [1], Hengyu Tan [1] Zhuohuan Li [1] and Yunfei Ma [2,*]

[1] College of Water Resources and Civil Engineering, China Agricultural University, Beijing, 100083, China

[2] Yantai Institute of China Agricultural University, Yantai, 264670, China

* Correspondence: Yunfeimayt@cau.edu.cn

Abstract

Double-sided solar greenhouses are recognized as energy-efficient agricultural facilities that significantly enhance land utilization and thermal performance through their unique double-sided lighting design, thereby promoting crop growth. However, challenges persist regarding insufficient heat storage capacity and suboptimal thermal environments within the shaded shed during the winter and spring seasons. To fully exploit the advantages of this greenhouse type, this study proposes a structural optimization methodology utilizing Computational Fluid Dynamics simulation. A CFD model was developed and validated against experimental data to ensure accuracy. Subsequently, the influence of key parameters, including roof geometry and wall thickness, on the internal photothermal environment was systematically analyzed. The results demonstrate that the 370 mm thick wall configuration achieves a daily peak temperature approximately 2°C lower than the 240 mm wall, indicating a more uniform spatial distribution, while exhibiting a nighttime temperature increase of up to 2.5°C, thereby confirming superior thermal insulation properties. Furthermore, the presence of a rear roof structure is critical for nighttime heat retention, maintaining a minimum temperature of approximately 5°C compared to 2°C in greenhouses lacking this feature, with a maximum temperature difference of 4.2°C, effectively optimizing temperature uniformity. Based on these findings, this research provides a robust theoretical foundation and technical support for the structural optimization of double-sided solar greenhouses and the advancement of facility agriculture.

Keywords: double-sided solar greenhouse; CFD simulation; spatial morphology optimization; photothermal environment; facility agriculture

1. Introduction

The double-slope solar greenhouse is a facility independently developed in China, evolving from the traditional solar greenhouse design. Structurally, it incorporates a rear greenhouse with a north-facing light-transmitting surface added to the north side of a traditional greenhouse. These two compartments share a common rear wall, forming the double-slope configuration. The south-facing compartment is termed the "Yangpeng," while the north-facing compartment is referred to as the "Yinpeng"。 The Yangpeng is primarily utilized for cultivating vegetables and flowers, whereas the Yinpeng is designated for crops tolerant to low temperatures and low light intensity, predominantly fungi. Consequently, this system facilitates seasonal production scheduling, enabling efficient year-round agricultural output [1–3].

Practical applications have demonstrated that double-slope solar greenhouses offer distinct advantages, including high land use efficiency, low construction costs, and superior comprehensive economic benefits. These facilities have been widely adopted in northern China, particularly in the Ningxia Hui Autonomous Region, Qinghai, and Inner Mongolia. Given their significant economic

 doi:10.20944/preprints202605.0411.v1

potential, further in-depth research is warranted [4]. Current literature primarily focuses on spatial morphology, envelope structure construction, and thermal environment analysis. For instance, Wu et al.[5] systematically analyzed the influence of multiple structural parameters of Chinese solar greenhouses on thermal performance. By integrating a greenhouse energy balance model with a detailed shape analysis, they developed a structural model to systematically evaluate the sensitivity of spatial morphology parameters—such as greenhouse span, ridge height, rear wall height, rear roof length, and lighting surface angle—to the thermal performance of the greenhouse. Their work provides a systematic theoretical basis for the optimal design of the spatial morphology of solar greenhouses.Fan et al.[6] investigated the system design and implementation methods for enhancing the application potential of Chinese solar greenhouses in cold desert regions. By integrating the selection of spatial morphology parameters with the optimization of enclosure structures, they explored strategies for improving the thermal performance of solar greenhouses under extreme climatic conditions. Han et al.[7] investigated a method for constructing the indoor thermal environment of Chinese solar greenhouses based on the heat storage and release characteristics of the north wall. They established a mathematical model that integrates simplified calculations of greenhouse spatial parameters with a phase-change heat storage wall. The study showed that using GH-20 composite phase-change heat storage wall panels could increase the solar contribution rate by 90.9%. Moreover, integrating multi-surface solar air collectors with dual-receiver tubes into the phase-change composite wall further increased the solar contribution rate to 95.4%, resulting in a more than 10% increase in winter cucumber yield. Xu et al. [8]conducted in-depth research on canopy heterogeneity analysis and light microclimate simulation of Chinese solar greenhouses. They employed three-dimensional modeling and numerical simulation methods to analyze the distribution patterns of the light environment inside the greenhouse, addressing the influence of greenhouse spatial morphology on light distribution and the refined simulation of the thermal environment.Additionally, Li and Zhang [9] explored the heat release dynamics of the shared wall, revealing that its heat storage capacity increases with wall height throughout the year. Furthermore, studies on cropping patterns suggest that a mushroom-vegetable rotation system yields the optimal economic benefits [10,11].

Among various environmental factors, temperature is one of the most critical determinants directly influencing the growth and development of vegetable crops. Currently, strategies for regulating the greenhouse thermal environment encompass both real-time monitoring via Internet of Things (IoT) systems and predictive simulation approaches [12–14]. With technological advancements, Computational Fluid Dynamics (CFD) has been proven to be an effective simulation tool in this field [15–17]. Due to its reliability and cost-effectiveness in predicting and analyzing greenhouse microclimates, CFD has been extensively utilized by numerous researchers [18–20]. At present, CFD is widely applied in studies concerning greenhouse environment regulation. For instance, Fernandez et al. [21] employed CFD to investigate the distribution patterns of environmental factors, such as temperature and humidity, within a tomato greenhouse, thereby facilitating environmental control. Lee et al. [22] examined ventilation and crop distribution, demonstrating that CFD can effectively evaluate the temperature field in semi-circular arch greenhouses. Joudi et al. [23] developed a dynamic model to analyze different soil depths, which was used to predict soil and air temperatures, significantly aiding greenhouse environmental management. Furthermore, Saberian et al. [24] utilized CFD to explore the dynamic temperature fields and solar heat loads under conditions of internal radiation and natural convection. Their study discussed ventilation and lighting requirements for greenhouses in hot seasons, providing practical guidance for regional greenhouse design.

Therefore, this study employs Computational Fluid Dynamics (CFD) to simulate the relationship between structural configurations and the thermal environment in double-slope solar greenhouses. By analyzing the effects of varying wall thicknesses and roof morphologies on the greenhouse thermal environment, this research aims to further elucidate the thermal characteristics

 doi:10.20944/preprints202605.0411.v1

of these structures. The findings will provide valuable references for crop production and the structural optimization of double-slope solar greenhouses.

2. Materials and methods

2.1. Experimental Greenhouse

The experimental double-slope solar greenhouse (Figure 1.) is located in Yantai, Shandong Province (121.43°N, 37.45°E). The greenhouse consists of a south span with a width of 10 m and a north span with a width of 6 m. The total length of the structure is 60 m, with a rear wall height of 3 m and a wall thickness of 0.37 m. The front roof of the sunny span is covered with polyvinyl chloride (PVC) film, and an insulated blanket is placed over the film. The insulated blanket was uncovered at 08:00 and covered at 16:00 daily. During the experimental period, the greenhouse was kept empty without any crop cultivation.

(a) (b)

(c)

Figure 1. (a) Field view of the shady span. **(b)** Field view of the sunny span. **(c)** Front view of the experimental double-slope solar greenhouse.

2.2. Measurement and Data Acquisition System

The experimental layout is illustrated in Figure 2. Nine temperature sensors were arranged along the north-south direction, as shown in Fig. 2a. Three cross-sections were established along the

 doi:10.20944/preprints202605.0411.v1

east-west direction; each section followed the same layout pattern as shown in Fig. 2b, resulting in a total of 27 temperature sensors. Data were recorded at 5-minute intervals.

The sensors used were the 179-T1L/179-THL temperature and humidity recorders, manufactured by Apresys (Shanghai) Precision Photoelectric Co., Ltd., with an operating temperature range of approximately -30°C to 70°C. Additionally, a weather station was installed outdoors to monitor environmental parameters, including air temperature, solar radiation intensity, and wind speed, in real-time.

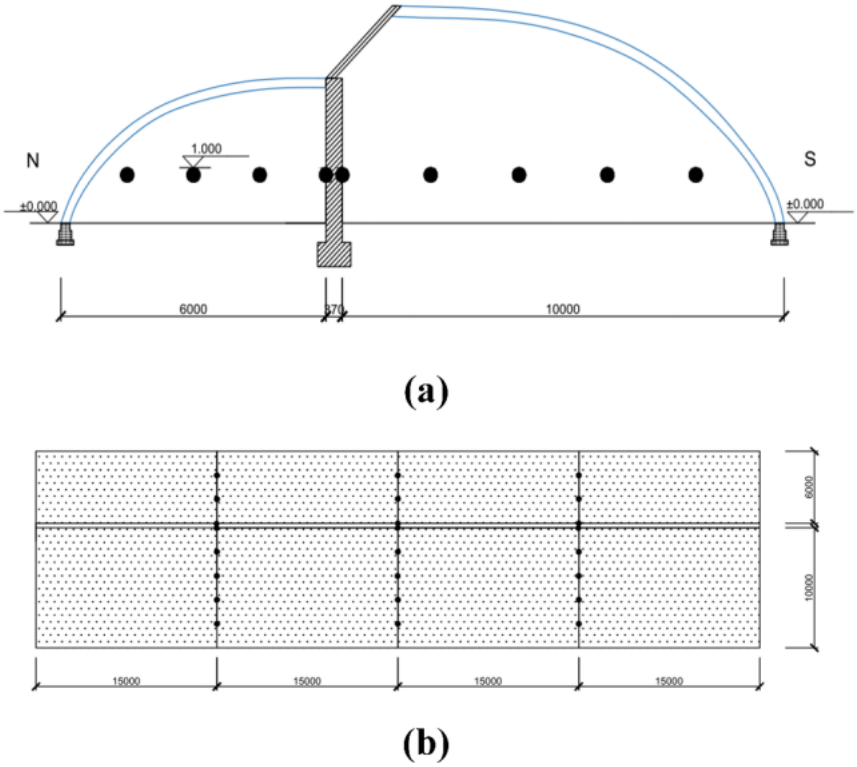

Figure 2. Layout of sensor nodes (Unit: mm). **(a)** Sensor layout along the north-south. **(b)** Sensor layout on the cross-section.

2.3. CFD Simulation

2.3.1. Construction of Greenhouse Geometric and Mesh Models

The computational fluid dynamics (CFD) geometric model of the solar greenhouse temperature environment was established using the SpaceClaim module in ANSYS, as shown in Figure 3. In the model, the negative Z-axis direction represents East, and the negative X-axis direction represents North. The model dimensions are identical to those of the actual solar greenhouse, with a soil thickness of 1 m. Subsequently, the model was imported into the ICEM module and discretized using a hexahedral-dominant mesh. The generated mesh is illustrated in Figure 4. A total of 1,070,164 nodes and 969,808 mesh elements were generated. The minimum mesh quality is 0.56, which meets the required mesh quality standards.

 doi:10.20944/preprints202605.0411.v1

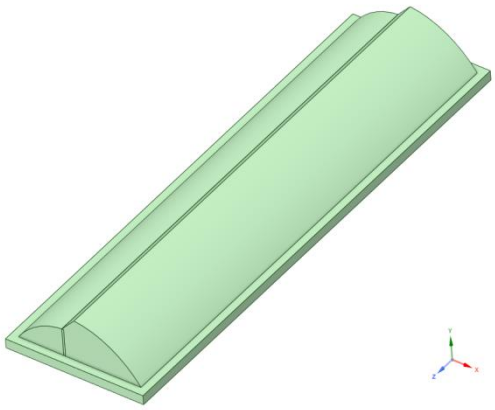

Figure 3. Three-dimensional model of the experimental double-sided solar greenhouse.

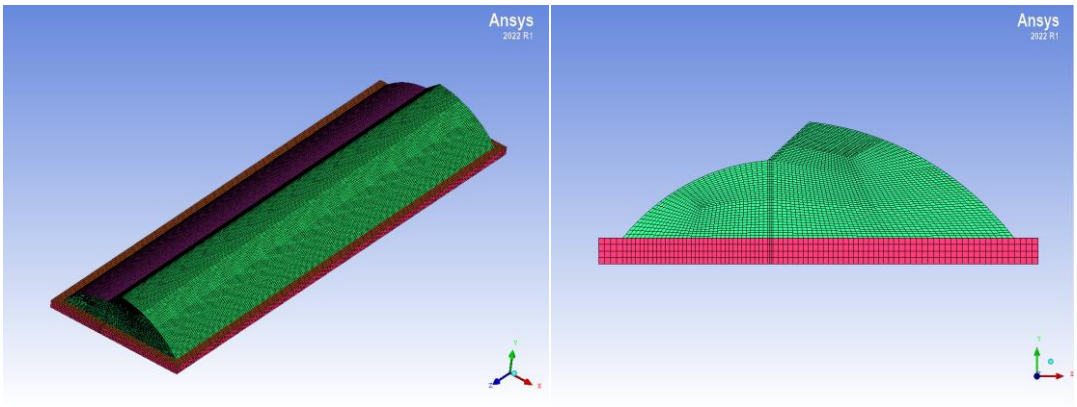

(a) (b)

Figure 4. Mesh generation of the experimental double-sided solar greenhouse.

2.3.2. Governing Equations

CFD technology is a discretized numerical method used to simulate fluid flow and heat transfer processes within a geometric domain. Its core consists of three fundamental conservation equations: mass, momentum, and energy conservation equations. Specifically, the partial differential equation for mass conservation indicates that the net mass flux flowing out of a control volume per unit time is equal to the mass loss generated by the density change within that control volume over the same time period.

$$\frac{\partial \rho}{\partial t} + \nabla \cdot (\rho \vec{v}) = S_m \quad (1)$$

Here,

ϱ represents the fluid density (kg/m³).

t represents time (s).

v represents the fluid velocity vector (m/s).

S_m represents the user-defined source term.

Fluid dynamics falls within the framework of classical mechanics; therefore, the applicability of the momentum conservation equation is fundamentally derived from Newton's Second Law. According to this law, the partial differential equation for momentum conservation can be described as follows: the rate of change of momentum of a fluid parcel is always equal to the vector sum of the external forces acting on it.

 doi:10.20944/preprints202605.0411.v1

$$\frac{\partial}{\partial t}(\rho\vec{v}) + \nabla \cdot (\rho\vec{v}\vec{v}) = -\nabla P + \nabla \cdot \bar{\bar{\tau}}_{\text{eff}} + \rho\vec{g} + \vec{F} \quad (2)$$

Here,

P represents the pressure on the fluid element (Pa).

$\bar{\bar{\tau}}_{\text{eff}}$ represents the stress tensor. and since the only body force acting on the control volume is gravity, $\vec{F}$=ϱ$\vec{g}$.

g represents the gravitational acceleration (m/s²).

The partial differential equation for energy conservation essentially characterizes the First Law of Thermodynamics. It indicates that the rate of energy increase within a control volume is equal to the heat flux received by the control volume plus the work done by body forces and surface forces acting on the control volume.

$$\frac{\partial}{\partial t}(\rho E) + \nabla \cdot \left(\vec{v}(\rho E + P)\right) = \nabla \cdot k_{\text{eff}} \nabla T - \sum_j h_j \overrightarrow{J_j} + \bar{\bar{\tau}}_{\text{eff}} \cdot \vec{v} + S_h \quad (3)$$

Here,

E represents the fluid energy (J).

k_{eff} represents the effective thermal conductivity (W/(m·K)).

T represents the temperature (K).

h_j represents the sensible enthalpy of the ideal gas (J/kg).

$\bar{\bar{\tau}}_{\text{eff}}$ represents the effective viscous shear stress.

$\overrightarrow{J_j}$ represents the species diffusion flux (kg/(m²·s)).

S_h represents the user-defined volumetric heat source term.

2.3.3. Turbulence Model

In nature, fluid flow is generally categorized into laminar flow and turbulent flow. The airflow within the double-sided solar greenhouse is considered to be turbulent. Researchers have utilized CFD to investigate various turbulence models for simulating greenhouse internal environments. However, it is important to note that no single universal model is suitable for all types of problems. The selection of a turbulence model requires a comprehensive consideration of multiple factors, including flow physics, the required level of accuracy, available computational resources, and simulation time.

In this study, a turbulence model was employed to calculate the internal gas flow of the experimental double-sided solar greenhouse. Through the comparison of different models within the CFD solver, the Realizable k-ε model was found to offer distinct advantages in terms of adaptability, wide applicability, and numerical stability. Consequently, the Realizable k-ε turbulence model was adopted in this study to simulate the environmental distribution within the double-sided solar greenhouse.

2.3.4. Radiation Model

To model the thermal radiation in a solar greenhouse, it is essential to determine a reliable radiation model. Researchers have used the Discrete Ordinates (DO) radiation model to calculate the heat transfer process caused by solar radiation passing through the transparent film of the solar greenhouse. The DO radiation model solves the Radiative Transfer Equation (RTE) to determine the spectral intensity radiation within the semi-transparent medium, thereby describing the coupled radiation and convection exchange in the greenhouse [25]. The DO radiation model can be directly applied to transparent, semi-transparent, and opaque optical media, such as air, film, glass, and soil

 doi:10.20944/preprints202605.0411.v1

surfaces. For the indoor air temperature in the greenhouse, the DO model demonstrates optimal accuracy [26]. Its governing equation is Eq. 4 [27].

$$\nabla(I(\vec{r},\vec{s})\vec{s})+(a_s+\sigma_s)I(\vec{r},\vec{s})=a_s n^2\frac{\sigma T^4}{\pi}+\frac{\sigma_s}{4\pi}\times\int_0^{4\pi} I\left(\vec{r},\vec{s'}\right)\phi\left(\vec{s},\vec{s'}\right)d\Omega \quad (4)$$

Here,

$\vec{r}$ is the position vector (m).

$\vec{s}$ is the direction vector.

I is the radiation intensity (W/m²).

which depends on position ($\vec{r}$) and direction ($\vec{s}$).

∇ is the divergence operator.

$\vec{s'}$ is the scattering direction vector.

a_s is the absorption coefficient (m^{-1}).

σ is the Stefan-Boltzmann constant (5.67×10^{-8} $W\cdot m^{-2}\cdot K^{-4}$).

σ_s is the scattering coefficient (m^{-1}).

n is the refractive index.

T is the temperature (K).

ϕ is the phase function.

Ω is the solid angle.

2.3.5. Assumptions in the Simulation Process

To facilitate the simulation analysis, the model was simplified under the premise of not compromising simulation fidelity and meeting accuracy requirements. The following assumptions were made:

(1) During the experiment, the test double-sided solar greenhouse was in a closed state, and natural ventilation within the greenhouse was negligible. Therefore, air exchange between the interior and exterior of the double-sided solar greenhouse was ignored.

(2) Since no crops were planted inside the double-sided solar greenhouse during the experiment, the effects of humidity and heat from plants were not considered.

(3) Due to the low moisture content in the soil and surrounding air of the double-sided solar greenhouse, latent heat exchange between them was neglected. Furthermore, the heat flux from the soil was significantly smaller than the heat flux flowing to the shared wall.

2.3.6. Boundary and Initial Condition Settings

In this study, a three-dimensional transient model was employed to simulate the dynamic changes of the microclimate within the solar greenhouse over time. The boundary conditions and initial conditions were determined based on experimental measurement data. Specifically, the experimental data measured on March 23, 2025, were selected for model construction.

The boundary conditions mainly included settings for the indoor and outdoor north and south roofs, soil, and north wall. From 8:00 to 16:00, the south roof was set as a layer of transparent plastic film, while for the remaining time, it was set as an insulation blanket. The outdoor temperature was applied to the external surface of the greenhouse envelope structure by programming a profile file.

The SIMPLE (Semi-Implicit Method for Pressure-Linked Equations) algorithm was selected for pressure-velocity coupling. In the calculation settings, the time step was set to 30 s, and the number of time steps was set to 2880. The parameters of the solar greenhouse envelope structure materials are shown in Table 1.

 doi:10.20944/preprints202605.0411.v1

Table 1. Parameters of the solar greenhouse envelope structure materials.

Material	Density (kg/m³)	Specific Heat Capacity (J/(kg·K))	Thermal Conductivity (W/(m·K))	Material Type
Air	1.225	1006.43	0.0242	Gas
Cement	2300	880	1.50	Opaque
Polystyrene Board	30	1380	0.042	Opaque
PVC Film	900	2550	0.290	Semi-transparent
Insulation Blanket	300	1275	0.11	Opaque
Indoor Soil	1600	2200	0.94	Opaque
Brick	1700	1050	0.760	Opaque
Polyurethane	40	1380	0.022	Opaque

2.3.7. Model Validation

Starting from 0:00 on March 23, 2025, the three-dimensional transient thermal environment of the solar greenhouse was simulated. The heat flux and temperature values at the experimental measuring points were extracted to validate the model. Here, the indoor air temperature is taken as an example to illustrate the model validation process.

Sensors were utilized to collect the air temperature values in the south chamber, which were then compared with the CFD-simulated air temperatures in the greenhouse, as shown in Figure 5. The calculation results indicate that the average relative error between the CFD simulation data and the measured data is 0.51%, and the maximum relative error is 0.94%. Among the 24 groups of data, 19 groups of deviation values fall within ±2℃, accounting for approximately 79.2%, demonstrating that the model accuracy meets the requirements.

 doi:10.20944/preprints202605.0411.v1

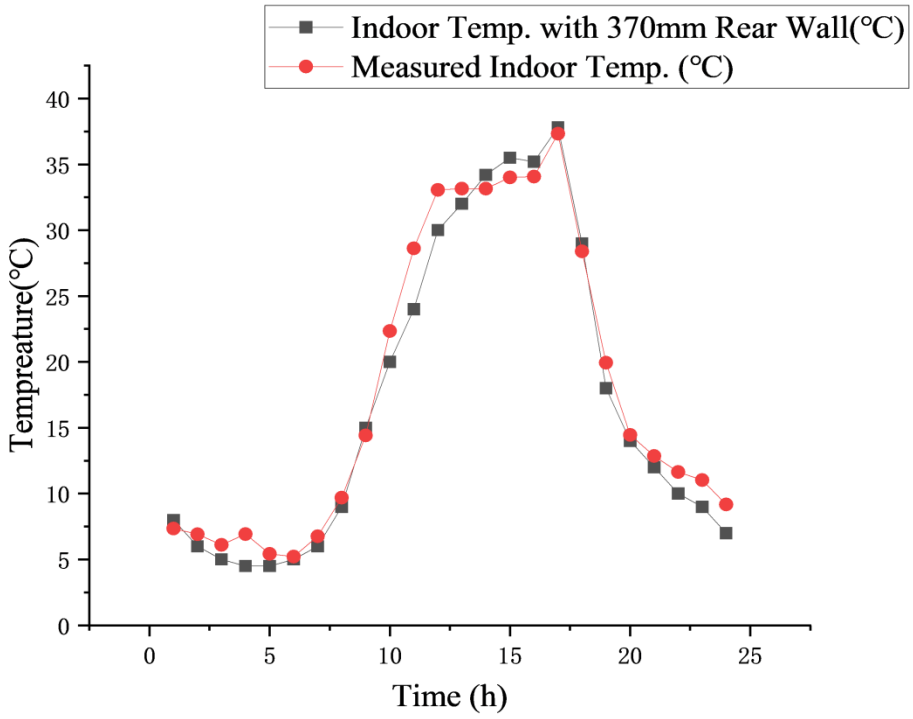

Figure 5. Temperature variation of the sunny shed (0:00–24:00): Comparison between the 370mm intermediate wall with rear roof and measured values.

2.4. Simulation Scheme

Following the aforementioned steps, a single-variable control strategy was implemented based on this model to simulate the variations in the indoor environment of different greenhouse types under identical environmental conditions. By comparing and analyzing the structures, the optimal spatial structure optimization scheme was selected. The specific workflow is illustrated in Figure 6., and the physical parameters of the simulated greenhouses are detailed in Table 2.

Table 2. Simulation parameters for different types of double-sided solar greenhouses.

 doi:10.20944/preprints202605.0411.v1

Group	Greenhouse No.	Span of Sunny Shed / m	Height of Shared Wall / m	Ridge Height / m	Wall Material
With Rear Roof	1	10	3	4.5	370 mm Cement Brick
	2	10	3	/	240 mm Cement Brick
Without Rear Roof	3	10	3	4.5	370 mm Cement Brick
	4	10	3	/	240 mm Cement Brick

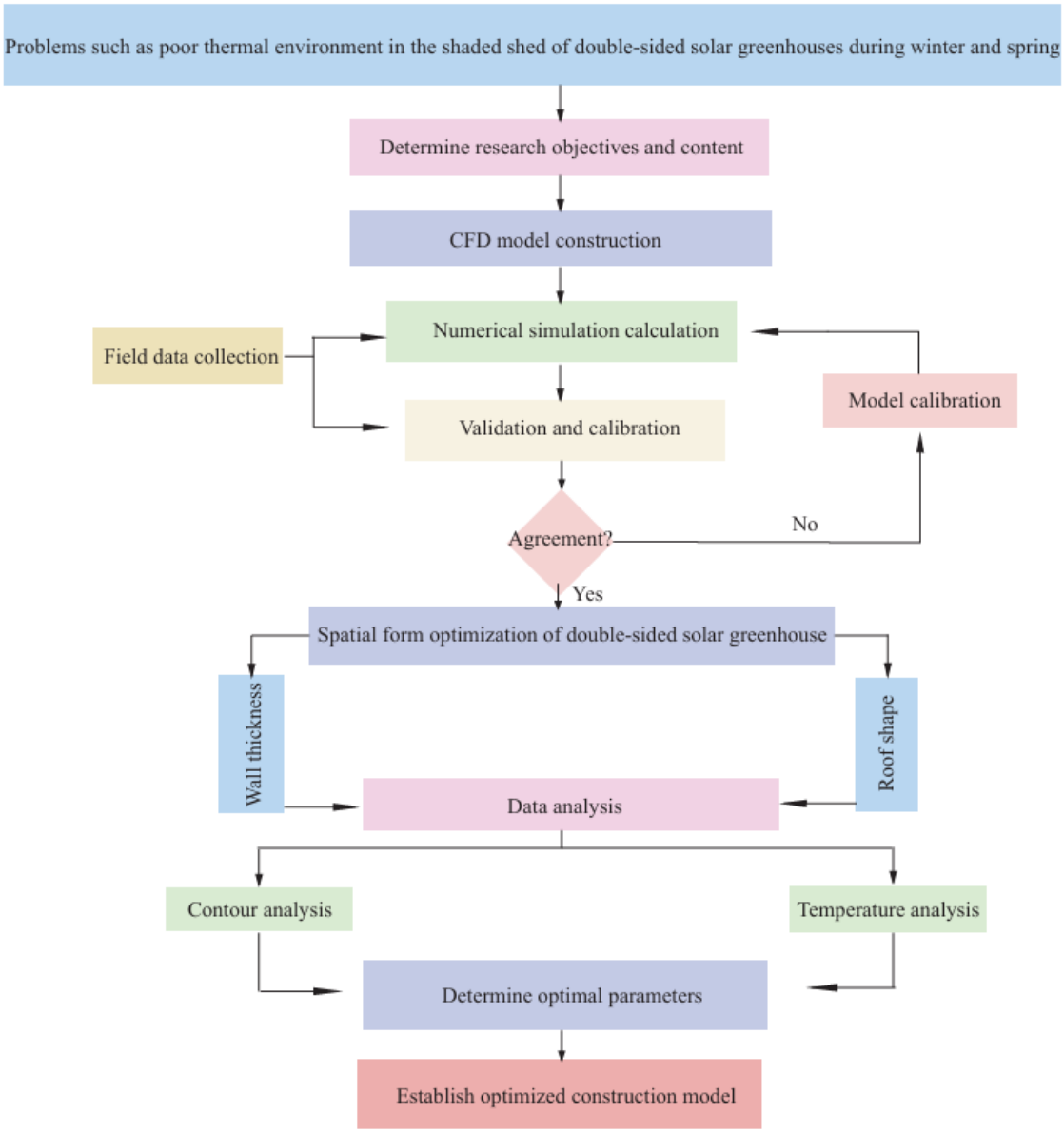

Figure 6. Research framework.

 doi:10.20944/preprints202605.0411.v1

3. Results and Discussion

3.1. Comparison and Analysis of Simulated Temperatures in Greenhouses with Different Wall Thicknesses

3.1.1. Temperature Comparison and Analysis of Greenhouses with Rear Roofs

Fig 7. and Fig 8. illustrate the temperature contours of the double-sided solar greenhouses with 370 mm intermediate walls (with and without rear roofs) at various time points: 1:00, 3:00, 5:00, 8:00, 10:00, 12:00, 14:00, 16:00, 18:00, 20:00, 22:00, and 24:00. The analysis reveals that the indoor temperature distributions of the two greenhouse types were similar during nighttime. However, Greenhouse 1 exhibited slightly higher temperatures near the ground, adjacent to the wall, and close to the roof compared to Greenhouse 2. This is attributed to the heat absorption during the day and subsequent release at night by the intermediate wall, indicating that the 370 mm thick intermediate wall possesses superior heat storage performance.

After the thermal blankets were uncovered from 8:00 to 16:00, Greenhouse 1 demonstrated a more pronounced and extensive temperature rise. However, around noon, the overall temperature in the greenhouse with the 370 mm wall was lower than that of the greenhouse with the 240 mm wall, and the temperature distribution was more uniform, avoiding localized overheating. This phenomenon may be due to the 240 mm wall reaching heat storage saturation earlier, rendering it unable to effectively absorb excess heat. Consequently, the surplus solar energy caused a rapid increase in indoor temperature, which could adversely affect crop growth if ventilation is not provided in time.

From 16:00 to 24:00, after the thermal blankets were covered, the cooling trends of both greenhouses showed little difference. Nevertheless, the temperature drop in Greenhouse 1 near the ground, wall, and roof was less significant than in Greenhouse 2. This observation suggests that the thicker 370 mm intermediate wall effectively retained heat within these specific zones.

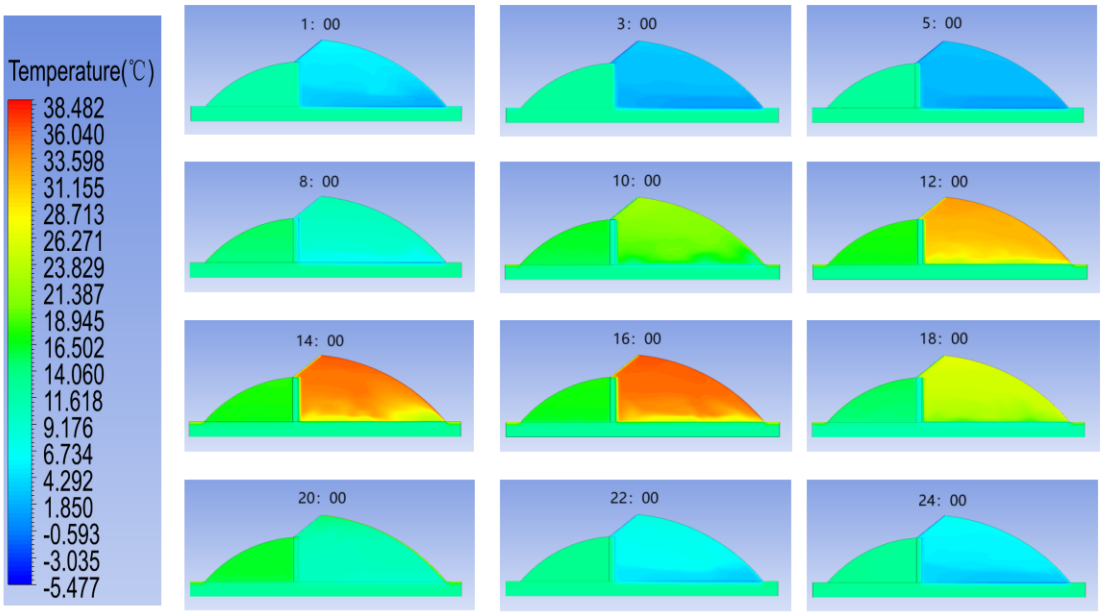

Figure 7. Greenhouse with a rear roof and a 370 mm intermediate wall.

 doi:10.20944/preprints202605.0411.v1

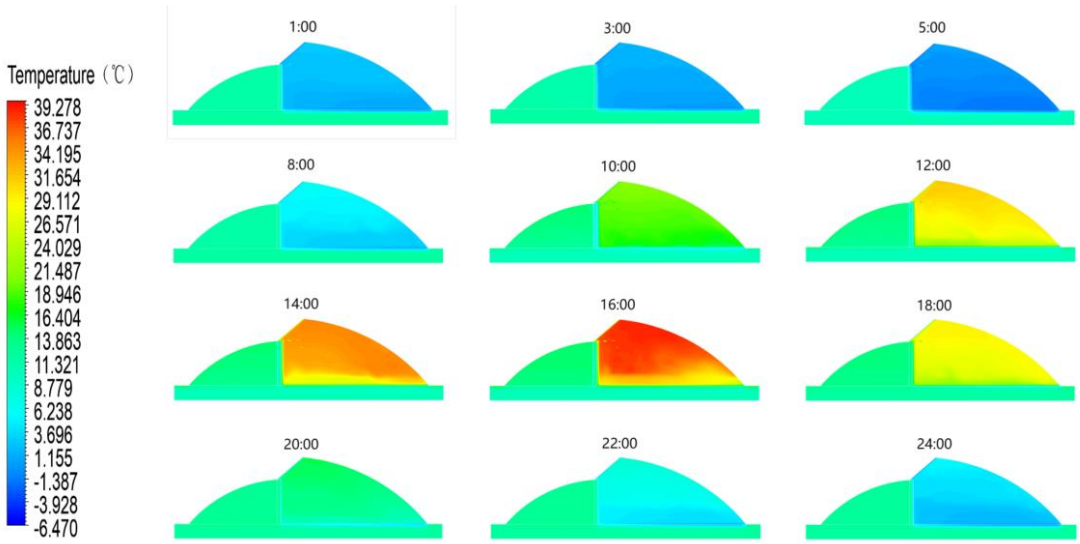

Figure 8. Greenhouse with a rear roof and a 240 mm intermediate wall.

Figure 9 illustrates the diurnal variation of air temperature in the sunny shed of greenhouses constructed with 370 mm and 240 mm cement brick intermediate walls over a 24-hour period (0:00–24:00). From 0:00 to 8:00, the nighttime temperatures of the two greenhouses showed little difference, with both exhibiting a downward trend. The temperature dropped rapidly in the early hours and subsequently stabilized with negligible fluctuations at lower levels; however, Greenhouse 1 consistently maintained slightly higher temperatures than Greenhouse 2. Between 8:00 and 16:00, both greenhouses experienced a warming trend. Greenhouse 2 exhibited a faster heating rate, surpassing Greenhouse 1 by approximately 2°C at 14:00, a difference that persisted until 16:00. This phenomenon is attributed to the lower heat capacity of the 240 mm intermediate wall, which results in a more rapid response to solar radiation. In contrast, the larger heat capacity of the 370 mm wall leads to a more gradual and sustained heat absorption and warming process. From 16:00 to 17:00, temperatures in both greenhouses continued to rise. Specifically, the temperature in Greenhouse 1 increased from 35.2°C to 37.81°C, while that in Greenhouse 2 rose from 37.86°C to 39.2°C. During the period from 17:00 to 24:00, both greenhouses entered a cooling phase. Greenhouse 1 demonstrated a slower cooling rate, resulting in a widening temperature gap after 19:00, with a maximum difference of 2.5°C.

 doi:10.20944/preprints202605.0411.v1

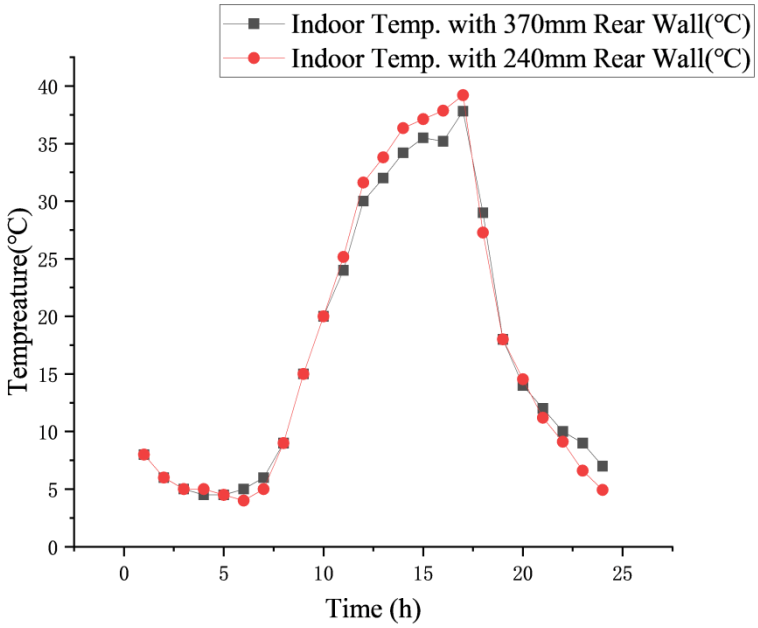

Figure 9. Diurnal variation of air temperature in the sunny shed of greenhouses with 370 mm and 240 mm intermediate walls (0:00–24:00).

3.1.2. Temperature Comparison and Analysis of Greenhouses without Rear Roofs

Figure 10 and Figure 11 illustrate the temperature contours of the double-sided solar greenhouses with 240 mm and 370 mm intermediate walls (without rear roofs) at various time points. The analysis indicates that the overall temperature difference between the two greenhouses from 0:00 to 8:00 was negligible, with both exhibiting low temperatures and insignificant fluctuations. Notably, this difference was smaller than that observed between the two greenhouse types with rear roofs.

After the thermal blankets were uncovered from 8:00 to 16:00, the shaded shed of Greenhouse 3 warmed up faster and maintained a generally higher temperature than that of Greenhouse 4; however, its sunny shed exhibited a slower heating rate. Around noon, Greenhouse 4 experienced localized overheating in certain areas. In contrast, the temperature distribution in the greenhouse with the 370 mm intermediate wall was more uniform.

From 16:00 to 24:00, after the thermal blankets were covered, the cooling trends of both greenhouses showed little difference. The shaded shed of Greenhouse 3 generally maintained higher temperatures than Greenhouse 4. Although low temperatures were observed near the ground in both, Greenhouse 3 exhibited slightly higher temperatures near the intermediate wall and roof compared to Greenhouse 4, indicating that the 370 mm thick intermediate wall possesses superior heat storage performance.

 doi:10.20944/preprints202605.0411.v1

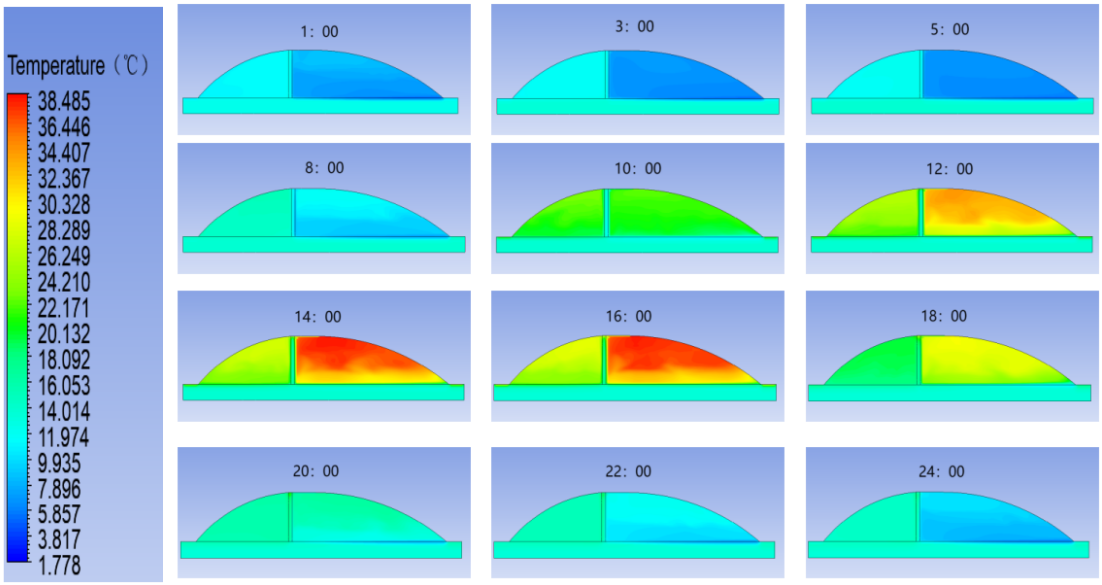

Figure 10. Greenhouse without a rear roof and with a 240 mm intermediate wall.

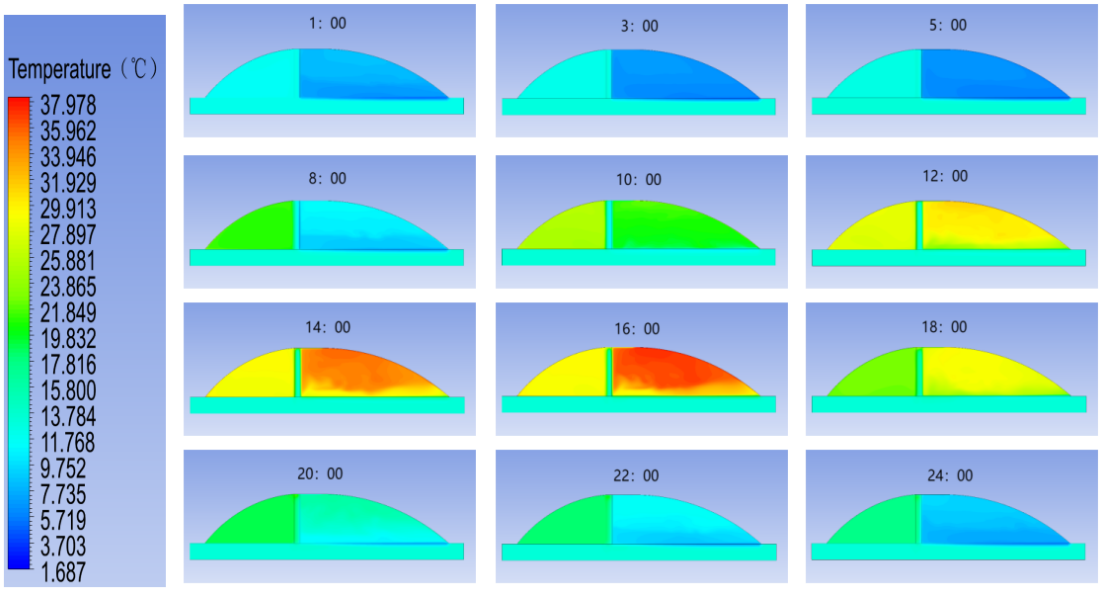

Figure 11. Greenhouse without a rear roof and with a 370 mm intermediate wall.

Figure 12. illustrates the diurnal variation of air temperature in the sunny shed of greenhouses without rear roofs, comparing those constructed with 370 mm and 240 mm cement brick intermediate walls over a 24-hour period (0:00–24:00). From 0:00 to 6:00, the temperature in the shaded shed of both greenhouses exhibited a downward trend. Greenhouse 3 cooled from 5.16°C to 1.13°C, while Greenhouse 4 cooled from 4.85°C to 1.02°C, showing negligible overall difference. Between 6:00 and 8:00, both greenhouses began to warm at a moderate rate; the temperature in Greenhouse 3 increased by 7.25°C, compared to a 6.58°C rise in Greenhouse 4. From 8:00 to 16:00, the heating rate accelerated for both greenhouses. Greenhouse 4 exhibited a slightly faster heating rate, reaching a peak temperature of 38°C at 15:00. In contrast, Greenhouse 3 demonstrated more stable heating, reaching a temperature of 36°C. During the period from 16:00 to 24:00, Greenhouse 3 experienced a more gradual cooling process. Starting at 20:00, its temperature exceeded that of Greenhouse 4 and remained higher until 24:00, whereas Greenhouse 4 exhibited larger temperature fluctuations. This phenomenon is attributed to the 370 mm intermediate wall storing a greater amount of heat during the day, which is released slowly and continuously after the thermal blankets are covered, thereby

 doi:10.20944/preprints202605.0411.v1

retarding the cooling rate. Conversely, the 240 mm wall stores less heat, leading to rapid heat loss and more pronounced temperature fluctuations once the insulation is in place.

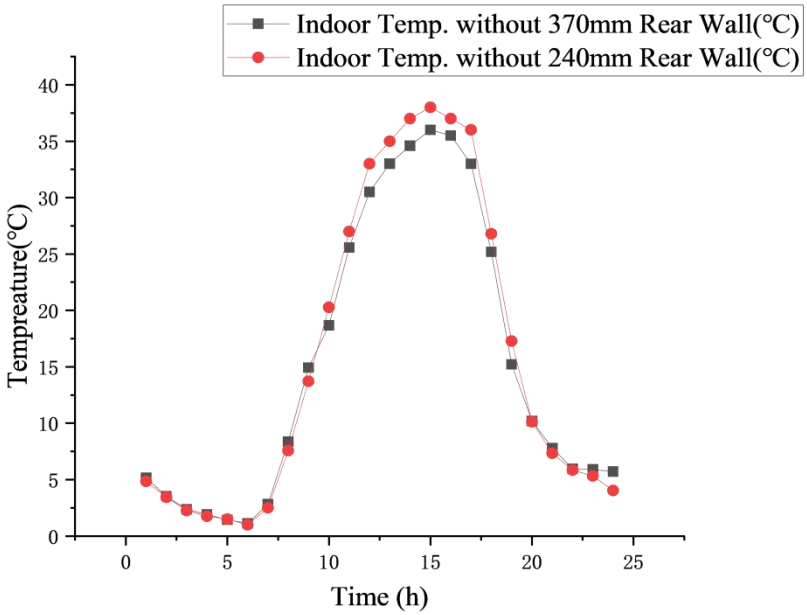

Figure 12. Diurnal variation of air temperature in the sunny shed of greenhouses without rear roofs featuring 370 mm and 240 mm intermediate walls (0:00–24:00).

3.2. Comparison and Analysis of Simulated Temperatures in Greenhouses with Different Roof Configurations

Figure 7. and Figure 11. display the temperature contours of solar greenhouses with 370 mm intermediate walls, comparing configurations with and without a rear roof across multiple time periods. The analysis reveals that from 0:00 to 8:00, the overall nighttime temperature of Greenhouse 1 (with rear roof) was significantly higher than that of Greenhouse 3 (without rear roof), with a more pronounced difference observed in the shaded shed. The greenhouse without a rear roof only exhibited temperatures comparable to the rear-roof model near the roof and ground surfaces; however, its lower shaded shed temperatures are unfavorable for crop growth. Although the distribution of low-temperature zones showed some similarities during certain periods, the greenhouse with a rear roof demonstrated superior temperature maintenance capabilities, continuously releasing heat accumulated during the day to stabilize the indoor environment.

From 8:00 to 16:00, after the thermal blankets were uncovered, the greenhouse without a rear roof exhibited a more rapid heating rate. This phenomenon is likely attributed to the wider coverage of PVC film and the larger light-transmitting surface area in the sunny shed. However, the greenhouse with a rear roof maintained a more uniform temperature distribution. Especially around noon, it featured a broader coverage of high-temperature zones with gentle gradient changes. In contrast, the temperature distribution in the greenhouse without a rear roof showed distinct regional disparities, with a sharp contrast between localized overheating and relatively cooler areas. These differences indicate that the presence of a rear roof not only aids in nighttime insulation but also optimizes heat distribution efficiency during the day, providing a more balanced thermal environment for crops in different zones, which is beneficial for growth consistency and quality control.

Between 16:00 and 24:00, following the covering of thermal blankets, the overall temperature of the greenhouses began to decline. However, Greenhouse 1 maintained higher overall temperatures and a slower cooling rate compared to Greenhouse 3. The greenhouse without a rear roof exhibited lower minimum temperatures and a more extensive low-temperature range. This is because the rear

 doi:10.20944/preprints202605.0411.v1

roof blocks top radiative heat loss; the heat it accumulates is released slowly, working in synergy with the heat emission from the intermediate wall to maintain internal temperatures and prevent the expansion of cold zones. Conversely, the greenhouse without a rear roof lacks structural obstruction at night, causing rapid heat loss through the top. While the intermediate wall retains heat, it can only sustain temperatures in its immediate vicinity and fails to support the thermal environment of the entire domain.

Figure 13. illustrates the diurnal variation of air temperature in the sunny shed for the double-sided asymmetric solar greenhouse with a rear roof and 370 mm intermediate wall versus the double-sided asymmetric greenhouse without a rear roof (0:00–24:00). The figure indicates that from 0:00 to 8:00, the sunny shed temperature in Greenhouse 1 was higher and more stable, with a minimum of approximately 5°C, whereas Greenhouse 3 dropped to a minimum of 2°C. From 8:00 to 16:00, the greenhouse with a rear roof experienced more stable warming. The greenhouse without a rear roof heated up faster, surpassing Greenhouse 1 at 11:00 and maintaining this lead until the thermal blankets were covered. At 16:00, immediately after covering, the temperature in the greenhouse with a rear roof rose from 35.2°C to 37.81°C within one hour, exceeding that of the greenhouse without a rear roof. From 17:00 to 24:00, both greenhouses began to cool. Greenhouse 3 cooled more rapidly, dropping to 5.96°C by 22:00, while Greenhouse 1 remained at 10°C. This is likely because the rear roof possesses thermal buffering and heat storage functions: it blocks radiative heat loss and slowly releases stored heat at night to retard cooling, while synergizing with the intermediate wall during the day to ensure stable and sustained warming.

In summary, the greenhouse with a rear roof and 370 mm intermediate wall exhibits a more uniform and higher overall indoor temperature distribution at night compared to the configuration without a rear roof. Although the overall temperature difference between the two configurations is not significant during the day, the greenhouse with a rear roof is more conducive to nighttime crop growth.

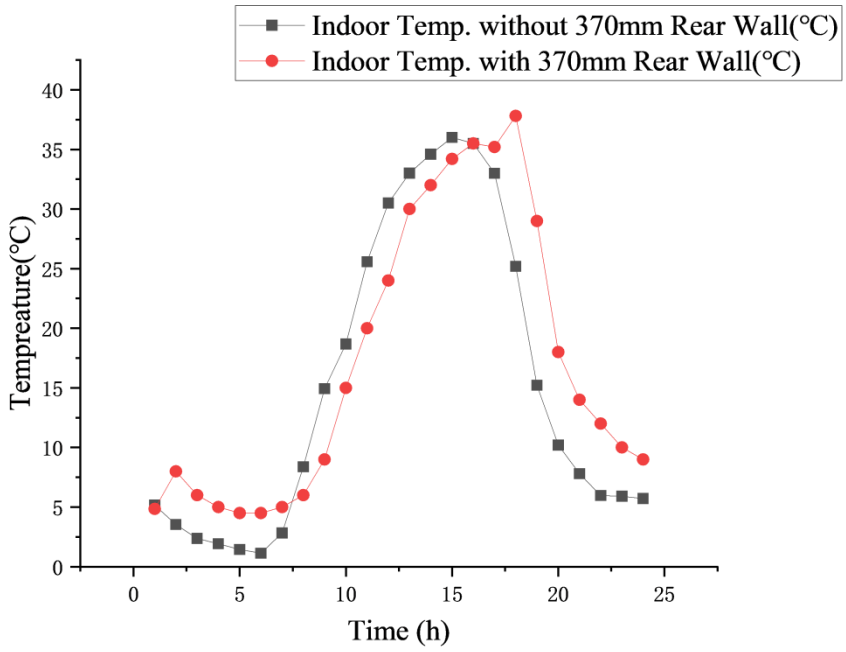

Figure 13. Diurnal variation of air temperature in the sunny shed of double-sided asymmetric greenhouses with 370 mm intermediate walls, comparing configurations with and without a rear roof (0:00–24:00).

 doi:10.20944/preprints202605.0411.v1

4. Discussion

4.1. The Rear Roof Acts as the Decisive Barrier for Nocturnal Insulation

The results unequivocally identify the rear roof structure as an indispensable "thermal barrier" within the microclimate of double-sided greenhouses, playing a critical role particularly during the nocturnal phase when heat dissipation is most acute. In cold regions, shading materials act as insulators that significantly reduce heat loss from greenhouses at night [28]. A comparative analysis of simulation data regarding the presence versus absence of a rear roof reveals that this structure significantly inhibits radiative heat loss from the upper sections. During the nighttime window (0:00–8:00), the minimum temperature in the shaded shed of the greenhouse equipped with a rear roof (Greenhouse 1) was maintained at approximately 5°C, whereas the minimum temperature in the greenhouse lacking this feature (Greenhouse 3) plummeted to 2°C, resulting in a substantial differential of 3°C.

The mechanism underpinning this phenomenon extends beyond the physical obstruction of direct radiation to the night sky. The rear roof functions as a thermal reservoir; the heat absorbed and stored during daylight hours is gradually released at night, creating a synergistic effect with the thermal release from the intermediate (wall body). This "dual heat source" mechanism effectively retards the cooling rate of the internal environment. The implementation of thermal storage–release systems within greenhouse envelopes has been demonstrated to reduce daytime high temperatures while releasing stored heat at night, achieving a warming effect of approximately 1–2 °C during nocturnal hours [29]. In northern regions such as Yantai, where nocturnal temperatures in winter and early spring are low, the presence of a rear roof dictates whether the shaded shed—typically utilized for cultivating cold-tolerant fungi or vegetables—can sustain temperatures above the biological zero point for crop growth. Consequently, the rear roof is not merely a shading structure but a decisive architectural element governing the stability of the nocturnal thermal environment.

4.2. Trade-Off Between Thermal Stability and Heating Rate Regarding Wall Thickness

The selection of wall thickness unveils a classic trade-off in greenhouse thermal performance: the conflict between thermal stability and the rate of temperature rise. Bendimerad et al. established a thermal analysis model to characterize the behavior of low-inertia polyethylene greenhouse walls, demonstrating that such structures exhibit reduced capacity to buffer diurnal temperature variations [30]. The study contrasts walls of 370 mm and 240 mm thickness, demonstrating that both exhibit distinct thermal responses throughout the diurnal cycle.

The greenhouse with the 240 mm wall exhibits a "rapid heating and rapid cooling" characteristic. During daylight hours (8:00–16:00), owing to its lower heat capacity, its heating rate is notably faster than that of the thick-walled greenhouse, with midday air temperatures exceeding those of the 370 mm wall greenhouse by approximately 2°C. However, this advantage rapidly transforms into a liability post-meridian; due to insufficient heat storage, the temperature drops precipitously at night, leading to violent fluctuations that are detrimental to crop physiology. This behavior aligns with the findings of Nishad and Krupa , who reviewed thermal energy storage strategies in greenhouses and emphasized that inadequate thermal mass exacerbates nocturnal temperature decline, compromising crop growth conditions during critical periods [31].

Conversely, the 370 mm wall, while sacrificing a fraction of the daytime heating velocity (resulting in a more gradual warming process), yields superior thermal stability. It absorbs and stores a greater magnitude of solar energy during the day, thereby mitigating local overheating at noon. At night, it functions as a massive "thermal battery," releasing heat slowly. Wang et al. further validated this "thermal battery" mechanism through a temperature-adaptive thermal storage/release wall system, demonstrating that optimized wall configurations effectively retard nighttime cooling rates and elevate nocturnal temperatures compared to conventional designs [32]. Data indicates that nocturnal temperatures in the 370 mm wall greenhouse are approximately 2.5°C higher than in the 240 mm variant. This "peak-shaving and valley-filling" capability demonstrates that for regions like

 doi:10.20944/preprints202605.0411.v1

Yantai with significant diurnal temperature ranges, increasing wall thickness is the most effective strategy for enhancing thermal inertia and dampening temperature fluctuations.

4.3. Structural Configuration Dictates the Uniformity of the Temperature Field

Beyond absolute temperature values, the influence of structural parameters on the "uniformity" of the internal temperature field is of paramount importance. The flow field cloud maps generated by CFD simulations intuitively display the regulatory effects of different structures on airflow organization and heat distribution.

The temperature fields in the thin-walled (240 mm) and rear-roof-less greenhouses often exhibit pronounced "zonal segmentation" and "localized overheating." For instance, in the absence of a rear roof, the lack of structural shading allows direct sunlight to create high-temperature zones, while shaded areas remain significantly cooler, resulting in a stark thermal contrast. Zhang et al. developed a CFD model to simulate temperature distributions in solar greenhouses, demonstrating that temperature stratification and non-uniformity were more obvious when the north wall was thinner, suggesting a desirable thickness of north wall for energy conservation [33]. Such non-uniform temperature fields can lead to the concurrent occurrence of "cold damage" and "heat stress" within the same facility, complicating environmental regulation.

In contrast, the greenhouse configured with a 370 mm thick wall and a rear roof (Greenhouse 1) exhibits a much more gradual internal temperature gradient. The combined action of thermal radiation from the thick wall and thermal insulation from the rear roof facilitates a more diffuse and uniform distribution of heat. Lu et al. further demonstrated through CFD-based optimization that airflow velocity and temperature distribution uniformity can be significantly improved by appropriate structural design, with temperature uniformity enhancements reaching 24.07% to 45.06% under optimized configurations [34]. This uniform temperature field not only minimizes variability in crop growth but also signifies a higher overall quality of the thermal environment, rendering it more conducive to the precision management required in modern facility agriculture.

4.4. Model Limitations and Future Development Trends and Challenges

Although this study successfully elucidated the thermal environment patterns of double-sided greenhouses via CFD modeling, with validation errors controlled within 0.94%, it is imperative to objectively acknowledge the model's limitations. Primarily, to simplify computations, the model assumed a completely hermetic greenhouse state, neglecting the influence of natural ventilation—a core mechanism for regulating temperature and humidity in actual production. Prior research has demonstrated that CFD-based natural ventilation simulations can effectively capture the effects of vent dimensions and positions on indoor airflow organization and temperature distribution, yet the integration of such mechanisms into predictive modeling remains constrained by computational demands and the need for detailed opening management data [35]. Furthermore, the model did not account for the existence of the crop canopy. Crops consume heat through transpiration (latent heat exchange) and alter airflow resistance, which inevitably leads to deviations between simulated air temperature and actual canopy temperature.As documented in the literature, the CFD modeling of greenhouse microclimates that accounts for the coupling of air transfers within the crop canopy—simulated as a porous medium exchanging momentum, heat, and mass with air—has been shown to significantly improve the accuracy of distributed climate predictions [36].

Looking ahead, the optimization of double-sided greenhouses faces a multitude of challenges and opportunities. On one hand, with the advent of Internet of Things (IoT) technologies, a key trend involves transitioning CFD simulation from a static "design tool" to a dynamic "real-time prediction tool," integrating real-time meteorological data for active environmental control. Recent advances in digital twin technology for smart greenhouses have demonstrated the feasibility of integrating real-time IoT sensing with predictive modeling, enabling remote monitoring and data-driven decision-making for environmental control [37]. On the other hand, while current research focuses primarily on geometric morphology and the physical properties of wall materials, future inquiries must more

 doi:10.20944/preprints202605.0411.v1

deeply couple "light-temperature-humidity-gas" multi-factor synergistic models and incorporate crop physiological responses (such as photosynthetic efficiency). As comprehensively summarized in the available literature, the implementation of CFD approaches that couple plant canopy activity with local microclimate modeling—including radiative transfers, transpiration, and photosynthetic activity—offers a promising pathway toward distributed climate predictions that capture crop-level physiological responses [38]. This represents a necessary shift from "structural optimization" to "precision optimization of the growth environment." For agricultural practices in Yantai and surrounding regions, the pressing task for facility agriculture engineering will be to further explore the potential of double-sided greenhouses in terms of land use efficiency and economic crop rotation, while simultaneously guaranteeing thermal insulation performance.

5. Conclusions

Based on the validated CFD model, this study conducted simulation analyses on double-sided solar greenhouses with varying wall thicknesses and configurations (with and without a rear roof on the sunny shed). The comparative analysis yielded the following conclusions:

(1) Prior to 06:00, increasing the thickness of the intermediate wall from 240 mm to 370 mm did not result in significant changes to the thermal environment of the sunny shed, regardless of the presence of a rear roof. However, the indoor temperature of the shaded shed increased during both daytime and nighttime periods with the thicker wall.

(2) The 240 mm thick intermediate wall demonstrated superior performance regarding heating efficiency and peak temperatures during daylight hours, with peak temperatures exceeding those of the 370 mm wall greenhouse by 2°C. Conversely, the 370 mm thick wall exhibited superior nocturnal insulation and thermal stability after dusk, with the temperature differential between the two wall thicknesses widening over time. The maximum temperature difference between greenhouses with varying wall thicknesses was 2.4°C for those with a rear roof and 1.67°C for those without.

(3) Greenhouses equipped with a rear roof maintained a more uniform and elevated overall indoor temperature distribution at night compared to those without. The maximum temperature difference for the 370 mm intermediate wall greenhouse was 4.2°C. Since overall temperatures during the day were comparable between the two configurations, the inclusion of a rear roof is more conducive to nocturnal crop growth.

(4) Comprehensive simulation results indicate that the combination of a 370 mm thick intermediate wall and a rear roof is the optimal configuration. This setup balances uniform daytime heating with sustained nocturnal insulation, making it particularly suitable for crop production in cold regions during winter and spring.

Significance of the Study

This study provides a theoretical basis and technical guidance for the optimization of structural parameters in double-sided solar greenhouses. By clarifying the thermal regulation mechanisms of wall thickness and rear roof configurations, the findings offer a scientifically optimized design solution for facility agriculture in cold regions, aiming to improve energy efficiency and ensure a stable thermal environment for crop production.

Author Contributions: Haoyue Wang: Writing – original draft, Literature research, Formal analysis, Software tool plotting, Writing – review & editing.**Hengyu Tan**: Writing – review & editing.**Zhuohuan Li**: Writing – review & editing.**Yunfei Ma**: Conceptualization, Formal analysis, Writing – review & editing, Supervision.

Funding: This research was funded by Yantai Science and Technology Bureau [2022XDRH002] and Yantai Municipal Education Bureau 2023 campus integration project [2023XDRHXMPT12].

Institutional Review Board Statement: Not applicable. .

Data Availability Statement: The data used in this study are available by contacting the corresponding author. .

 doi:10.20944/preprints202605.0411.v1

Conflicts of Interest: The authors declare no conflicts of interest.

Reference

1. Yang, X.; Ma, Y. Design and Thermal-Optical Environment Simulation of Double-Slope Greenhouse Roof Structure Based on Ecotect. *Agric.-Basel* **2024**, *14*, doi:10.3390/agriculture14081410.
2. Ma, Y.; Li, X.; Fu, Z.; Zhang, L. Structural Design and Thermal Performance Simulation of Shade Roof of Double-Slope Greenhouse for Mushroom-Vegetable Cultivation. *Int. J. Agric. Biol. Eng.* **2019**, *12*, 126–133, doi:10.25165/j.ijabe.20191203.4852.
3. Liu, J.; Liang, D.; Ma, Y. Thermal Environment Simulation and Analysis of Renovated Solar Greenhouses with Enhanced Cultivation Area and Space. *PLOS One* **2025**, *20*, doi:10.1371/journal.pone.0335954.
4. Wei XiaoMing, W.X.; Zhou ChangJi, Z.C.; Cao Nan, C.N.; Sheng BaoYong, S.B.; Chen SongYun, C.S.; Lu ShaoWei, L.S.; Wei, X.M.; Zhou, C.J.; Cao, N.; Sheng, B.Y.; et al. Evolution of Structure and Performance of Chinese Solar Greenhouse. *Jiangsu J. Agric. Sci.* **2012**, *28*, 855–860.
5. Wu, X.; Li, Y.; Jiang, L.; Wang, Y.; Liu, X.; Li, T. A Systematic Analysis of Multiple Structural Parameters of Chinese Solar Greenhouse Based on the Thermal Performance. *Energy* **2023**, *273*, doi:10.1016/j.energy.2023.127193.
6. Fan, Z.; Liu, Z.; Li, Y.; Zhang, J.; Tu, G.; Ding, T. New Insights to Boost the Application Potential of Chinese Solar Greenhouses in Cold Desert Regions: System Design and Implementation. *Energy* **2024**, *313*, doi:10.1016/j.energy.2024.133921.
7. Han, F.; Chen, C.; Chen, H.; Duan, S.; Lu, B.; Jiao, Y.; Li, G. Research on Creating the Indoor Thermal Environment of the Solar Greenhouse Based on the Solar Thermal Storage and Release Characteristics of Its North Wall. *Appl. Therm. Eng.* **2024**, *241*, doi:10.1016/j.applthermaleng.2024.122348.
8. Xu, D.; Chen, H.; Ji, F.; Zhu, J.; Wang, Z.; Zhang, R.; Hou, M.; Huang, X.; Wang, D.; Lu, T.; et al. New Insights on Canopy Heterogeneous Analysis and Light Micro-Climate Simulation in Chinese Solar Greenhouse. *Comput. Electron. Agric.* **2025**, *233*, doi:10.1016/j.compag.2025.110179.
9. Li, L.; Zhang, Y. Combining Light with Shade Solar Greenhouses Wall of Different Season Shared Combustion Status. *North. Hortic.* **2010**, *15*, 80–84.
10. Wang, G.; Liu, F.; Liu, H. Yinyang Type Solar Greenhouse Facilities Construction and Cultivation Mode. *China Veg.* **2009**, *15*, 44–45.
11. Li, L. Comparative Analysis of the Environmental Characteristics of Shade Solar Greenhouses and the Growth of Red Earth Grapes. Doctoral dissertation, Master dissertation. Yinchuan: Ningxia University, 2010.
12. Reichrath, S.; Davies, T.W. Using CFD to Model the Internal Climate of Greenhouses: Past, Present and Future. *Agronomie* **2002**, *22*, 3–19, doi:10.1051/agro:2001006.
13. Sase, S.; Takakura, T.; Nara, M. Wind Tunnel Testing on Airflow and Temperature Distribution of a Naturally Ventilated Greenhouse. In Proceedings of the III International Symposium on Energy in Protected Cultivation 148; 1983; pp. 329–336.
14. Boulard, T.; Kittas, C.; Roy, J.C.; Wang, S. SE—Structures and Environment: Convective and Ventilation Transfers in Greenhouses, Part 2: Determination of the Distributed Greenhouse Climate. *Biosyst. Eng.* **2002**, *83*, 129–147, doi:10.1006/bioe.2002.0114.
15. Okushima, L.; Sase, S.; Nara, M. A Support System for Natural Ventilation Design of Greenhouses Based on Computational Aerodynamics. In Proceedings of the International Symposium on Models for Plant Growth, Environmental Control and Farm Management in Protected Cultivation 248; 1988; pp. 129–136.
16. Baxevanou, C.; Fidaros, D.; Bartzanas, T.; Kittas, C. Numerical Simulation of Solar Radiation, Air Flow and Temperature Distribution in a Naturally Ventilated Tunnel Greenhouse. *Agric. Eng. Int.: CIGR J.* **2010**, *12*, 48–67.
17. Mistriotis, A.; Bot, G.P.A.; Picuno, P.; Scarascia-Mugnozza, G. Analysis of the Efficiency of Greenhouse Ventilation Using Computational Fluid Dynamics. *Agric. For. Meteorol.* **1997**, *85*, 217–228, doi:10.1016/S0168-1923(96)02400-8.

 doi:10.20944/preprints202605.0411.v1

18. Short, T.H.; Lee, I. Temperature and Airflow Predictions for Multi-Span Naturally Ventilated Greenhouse. In Proceedings of the International Symposium on Design and Environmental Control of Tropical and Subtropical Greenhouses 578; 2001; pp. 141–152.
19. Lee, I.-B.; Bitog, J.P.P.; Hong, S.-W.; Seo, I.-H.; Kwon, K.-S.; Bartzanas, T.; Kacira, M. The Past, Present and Future of CFD for Agro-Environmental Applications. *Comput. Electron. Agric.* **2013**, *93*, 168–183, doi:10.1016/j.compag.2012.09.006.
20. Norton, T.; Sun, D.-W.; Grant, J.; Fallon, R.; Dodd, V. Applications of Computational Fluid Dynamics (CFD) in the Modelling and Design of Ventilation Systems in the Agricultural Industry: A Review. *Bioresour. Technol.* **2007**, *98*, 2386–2414, doi:10.1016/j.biortech.2006.11.025.
21. Fernandez, J.E.; Bailey, B.J. The Influence of Fans on Environmental Conditions in Greenhouses. *J. Agric. Eng. Res.* **1994**, *58*, 201–210, doi:10.1006/jaer.1994.1049.
22. Lee, I.-B.; Short, T.H. Two-Dimensional Numerical Simulation of Natural Ventilation in a Multi-Span Greenhouse. *Trans. ASAE* **2000**, *43*, 757–753.
23. Joudi, K.A.; Farhan, A.A. A Dynamic Model and an Experimental Study for the Internal Air and Soil Temperatures in an Innovative Greenhouse. *Energy Convers. Manage.* **2015**, *91*, 76–82, doi:10.1016/j.enconman.2014.11.052.
24. Saberian, A.; Sajadiye, S.M. The Effect of Dynamic Solar Heat Load on the Greenhouse Microclimate Using CFD Simulation. *Renewable Energy* **2019**, *138*, 722–737, doi:10.1016/j.renene.2019.01.108.
25. Bournet, P.E.; Khaoua, S.A.O.; Boulard, T. Numerical Prediction of the Effect of Vent Arrangements on the Ventilation and Energy Transfer in a Multi-Span Glasshouse Using a Bi-Band Radiation Model. *Biosyst. Eng.* **2007**, *98*, 224–234, doi:10.1016/j.biosystemseng.2007.06.007.
26. Liu, W.; Qu, M.; Zhang, F.; Cao, S.; Li, Z.; Xu, Z. A Comparative Study of Thermal Radiation Model in Chinese Solar Greenhouse. *PLOS One* **2024**, *19*, doi:10.1371/journal.pone.0309225.
27. Bournet, P.-E.; Rojano, F. Advances of Computational Fluid Dynamics (CFD) Applications in Agricultural Building Modelling: Research, Applications and Challenges. *Comput. Electron. Agric.* **2022**, *201*, doi:10.1016/j.compag.2022.107277.
28. Ahemd, H.A.; Al-Faraj, A.A.; Abdel-Ghany, A.M. Shading Greenhouses to Improve the Microclimate, Energy and Water Saving in Hot Regions: A Review. *Sci. Hortic.* **2016**, *201*, 36–45, doi:10.1016/j.scienta.2016.01.030.
29. Wang, X.; Sun, G.; Zhang, L.; Lei, W.; Zhang, W.; Li, H.; Zhang, C.; Guo, J. Application of Green Energy in Smart Rural Passive Heating: A Case Study of Indoor Temperature Self-Regulating Greenhouse of Winter in Jinan, China. *Energy* **2023**, *278*, doi:10.1016/j.energy.2023.127770.
30. Bendimerad, S.; Mahdjoub, T.; Bibi-Triki, N.; Bessenouci, M.Z.; Draoui, B.; Bechar, H. Simulation and Interpretation of the BIBI Ratio CB (.), as a Function of Thermal Parameters of the Low Inertia Polyethylene Wall of Greenhouses. In Proceedings of the 8TH INTERNATIONAL CONFERENCE ON MATERIAL SCIENCES, CSM8-ISM5; Hamieh, T., Ed.; Elsevier Science Bv: Beirut, LEBANON, 2014; Vol. 55, pp. 157–164.
31. Nishad, S.; Krupa, I. Phase Change Materials for Thermal Energy Storage Applications in Greenhouses: A Review. *Sustainable Energy Technol. Assess.* **2022**, *52*, doi:10.1016/j.seta.2022.102241.
32. Wang, H.; Zhang, X.; Wang, R. Temperature Adaptive Thermal Storage/Release Wall Based on Dynamic Spectral Control. *Energy Build.* **2025**, *326*, doi:10.1016/j.enbuild.2024.115041.
33. Zhang, X.; Wang, H.; Zou, Z.; Wang, S. CFD and Weighted Entropy Based Simulation and Optimisation of Chinese Solar Greenhouse Temperature Distribution. *Biosyst. Eng.* **2016**, *142*, 12–26, doi:10.1016/j.biosystemseng.2015.11.006.
34. Lu, J.; Li, H.; Wang, C.; Tian, X.; Song, W.; Zhao, S.; Wang, K. CFD Based Airflow Uniformity Optimization of Chinese Solar Greenhouses with Long-Row Cultivation: Impact of Unit Layout Design. *Case Stud. Therm. Eng.* **2025**, *71*, doi:10.1016/j.csite.2025.106192.
35. Benni, S.; Tassinari, P.; Bonora, F.; Barbaresi, A.; Torreggiani, D. Efficacy of Greenhouse Natural Ventilation: Environmental Monitoring and CFD Simulations of a Study Case. *Energy Build.* **2016**, *125*, 276–286, doi:10.1016/j.enbuild.2016.05.014.

 doi:10.20944/preprints202605.0411.v1

36. Fatnassi, H.; Bournet, P.E.; Boulard, T.; Roy, J.C.; Molina-Aiz, F.D.; Zaaboul, R. Use of Computational Fluid Dynamic Tools to Model the Coupling of Plant Canopy Activity and Climate in Greenhouses and Closed Plant Growth Systems: A Review. *Biosyst. Eng.* **2023**, *230*, 388–408, doi:10.1016/j.biosystemseng.2023.04.016.
37. Rahman, H.; Shah, U.M.; Riaz, S.M.; Kifayat, K.; Moqurrab, S.A.; Yoo, J. Digital Twin Framework for Smart Greenhouse Management Using Next-Gen Mobile Networks and Machine Learning. *Future Gener. Comput. Syst.-Int. J. Escience* **2024**, *156*, 285–300, doi:10.1016/j.future.2024.03.023.
38. Boulard, T.; Roy, J.-C.; Pouillard, J.-B.; Fatnassi, H.; Grisey, A. Modelling of Micrometeorology, Canopy Transpiration and Photosynthesis in a Closed Greenhouse Using Computational Fluid Dynamics. *Biosyst. Eng.* **2017**, *158*, 110–133, doi:10.1016/j.biosystemseng.2017.04.001.